






RESEARCH ARTICLE | OCTOBER 12 2023

Enhancing the quality of amplitude patterns using time-multiplexed virtual acoustic fields

Sonia Elizondo ; Iñigo Ezcurdia ; Jaime Goñi ; Mikel Galar ; Asier Marzo H 

<https://doi.org/10.1063/5.0164657>

This article may be downloaded for personal use only. Any other use requires prior permission of the author and AIP Publishing.

The following article appeared in Sonia Elizondo, Iñigo Ezcurdia, Jaime Goñi, Mikel Galar, Asier Marzo; Enhancing the quality of amplitude patterns using time-multiplexed virtual acoustic fields. *Appl. Phys. Lett.* 9 October 2023; 123 (15): 154102. <https://doi.org/10.1063/5.0164657> and may be found at <https://doi.org/10.1063/5.0164657> .

Enhancing the quality of amplitude patterns using time-multiplexed virtual acoustic fields

doi: [10.1063/5.0164657](https://doi.org/10.1063/5.0164657) Submitted: 23 June 2023 · Accepted: 2 October 2023

Published Online: 12 October 2023

Sonia Elizondo,  Iñigo Ezcurdia,  Jaime Goñi,  Mikel Galar,  and Asier Marzo^{a)} 

AFFILIATIONS

Universidad Pública de Navarra, Departamento de Estadística, Informática y Matemáticas, Pamplona, Spain

^{a)}Author to whom correspondence should be addressed: asier.marzo@unavarra.es

ABSTRACT

Ultrasonic fields can push and levitate particles, heat up materials, induce contactless tactile stimuli, or affect the blood-brain barrier. Current phased-arrays can create dynamic amplitude patterns, but their quality may be insufficient due to the limited density of emitters. On the other hand, passive modulators can provide high quality, but only static patterns can be generated. Here, we show and evaluate how the average of multiple time-multiplexed amplitude fields improves the resolution of the obtained patterns when compared with the traditional single-emission method. We optimize the non-linear problem of decomposing a target amplitude field into multiple fields considering the limitations of the phased-array. The presented technique improves the quality for existing setups without modifying the equipment, having the potential to improve bio-printing, haptic devices, or ultrasonic medical treatments.

<https://doi.org/10.1063/5.0164657>

Custom acoustic fields are employed in particle,^{1,2} aerosol³ or cell⁴ patterning; as well as for ablation of tumors,⁵ Alzheimer treatment,⁶ or tactile stimuli.⁷ Consequently, being able to generate fields with custom patterns can significantly advance the fields of bio-printing or medical ultrasound.

Acoustic fields can be dynamically shaped to specific patterns by using phased-arrays composed of various emitters with controllable amplitude and phases.^{8,9} These arrays can generate different amplitude fields by electronically adjusting the signal of each emitter, but the resulting fields lack quality given the limited number of emitters, which are usually larger than half a wavelength ($k/2$). Using a phased-array to generate amplitude patterns has been achieved by adapting the Gerchberg–Saxton algorithm to consider the limited number of emitters that current devices have⁸ or by optimizing the emissions of each emitter to obtain target patterns.⁹ However, the obtained patterns were limited in resolution given the low number of emitters (16×16 elements of 1.16 k in size, or 20×20 elements). Available phased-arrays with enough power for patterning or manipulation usually have this resolution.

On the other hand, passive modulators can be manufactured with a high resolution,^{1,2,10–14} for example on the order of 120×120 elements,¹ but they are static and generate only one pattern. These passive structures can modulate impinging waves to obtain high quality patterns,¹ but they are static and one plate is needed per target pattern. Some improvements allow to produce different fields when the modulator is impinged by different

frequencies,¹⁵ but the number is limited to 2 or 3 fixed patterns, or to 6 with losses on the accuracy.¹⁶

Combinations of phased-arrays and passive modulators provide some flexibility over the static patterns. Cox *et al.*¹⁷ used this combination for focusing along the vertical direction a trap generated with the array and enhanced its trapping performance on a single particle. Athanassiadis *et al.*¹⁸ were able to code ten patterns in stacked passive modulators, these patterns were projected when impinged by one of the ten different emitters that were behind the modulator, yet only a fixed amount of patterns were encoded in the modulator with some loss in their resolution.

Time multiplexation consists in rapidly switching the emitted fields. Time multiplexation has been explored for particle manipulation by switching between two modes in a microfluidic channel to control the horizontal position of the particles.¹⁹ Virtual vortices²⁰ are pairs of vortices that rapidly switch their topological charge to cancel their orbital angular momentum and stably trap particles larger than the wavelength. Rapidly switching between a standing-wave and a twin-trap led to an acoustic lock,²¹ a trap that holds sub-wavelength asymmetric objects in position and orientation. Three different predefined fields can be switched quickly to combine their radiation forces in particle manipulation,²² also multiple traps can be quickly multiplexed in time to trap various particles.^{23–25} However, all of these methods are focused on controlling the forces at specific points to trap particles and cannot generate complex 2D patterns. Furthermore, the

multiplexed fields were predefined by the researchers, not obtained through decomposition or optimization.

Here, we present a technique to calculate multiple fields that can be emitted by an array that, when averaged in amplitude, result in a virtual field that has more quality than any single-emission field that can be produced with the same array. To achieve this, we optimize the non-linear problem of decomposing a target amplitude field into multiple fields that can be emitted with a phased-array. When the amplitude of these fields is averaged, they approximate the target field. This technique improves the quality of the resulting amplitude fields without the need of modifying existing hardware, being applicable to existing systems, and also to upcoming higher resolution arrays, e.g., high-power arrays that have more than 20×20 emitters.

The target amplitude field is a real 2D matrix, which is flattened into a 1D vector named `targetField`. On the other hand, `virtualField` is the average of the amplitude of the composing multiplexed fields, i.e., $\text{virtualField} = (|\text{multiplexed}_1| + \dots + |\text{multiplexed}_m|)/m$. Here, multiplexed_j is a complex field (flattened into a vector as well) that results from the matrix multiplication of an emission vector e_j and the propagators matrix P , that is, $\text{multiplexed}_j = e_j P$ where $j = 1 \dots m$ for the different multiplexed fields and emission vectors. A given emission vector e_j contains one complex number per emitter, and the emitter emission is encoded as $(amp e^{i\phi})$, where amp is the amplitude and ϕ is the phase. Note that the propagators matrix P remains the same for all the multiplexed fields since the emitters and the target field points do not change position.

A given value p_{mn} from the propagators matrix P represents the complex propagator from the position of emitter m to the target point n and can be pre-calculated using for example the Piston Model²⁶ $p_{mn} = A_0 \frac{D(h)}{d} e^{i(kd)}$, where A_0 is the power constant of the emitter, d is the distance between the center of the emitter m and the point in the field n , $k = 2\pi/\lambda$ is the wavenumber, λ is the wavelength, and $D(h)$ is the directivity function of the emitter that depends on the angle h

between the emitter normal and the point n . The directivity function of a vibrating piston source can be expressed as $D(h) = 2J_1(ka \sin h) / ka \sin h$, where J_1 is a first order Bessel function of the first kind and a is the radius of the piston.

As such, the loss function to minimize is the mean squared error (MSE) between the `virtualField` and the `targetField` as a function of the emission vectors for each of the multiplexed fields $O(e_1, \dots, e_m) = MSE(\text{virtualField}, \text{targetField})$. Other loss functions were tested (see supplementary material Fig. 1) but MSE provided the best general results. In Fig. 1, we show a single-emission field, multiplexed fields, and the resulting virtual field. It can be seen that the decomposition of a virtual field is not trivial. These examples are, respectively, from the circular array and the square array, both described later on in the paper.

We used a quasi-newton gradient-descent optimizer (*fminunc* function from Matlab R2019b) with numerical approximation of the gradient and default parameters. In general, 40 iterations were enough to converge into a solution. Different executions of the optimization produced different phase values, but the obtained value (MSE in this case) was similar. Meaning that although there are local minima, they provide equally good solutions. An Adam optimizer with autodiff (Tensorflow 2.11, learning rate = 0.1, 400 iterations) provided similar results. The optimization was unconstrained since phase is cyclical, Phases $[-\pi, \pi]$ were initialized randomly with a uniform distribution and amplitudes were fixed to 1. Amplitude modulation is discussed at the end of the article.

For both simulations and experiments, we selected two ultrasonic arrays. First, a circular array with 64 emitters of 1.6 cm (1.9 k) diameter divided into two overlapping circumferences of 32 emitters each, all pointing toward the center of the array, the radius of the array was 12 cm (14k). Second, a square array of 16×16 emitters of 1 cm (1.16k) diameter. The array had 16 cm of side (18.6 k). The fields were generated 20 cm above the square array (*TargetField* of $10 \times 10 \text{ cm}^2$) and at the center of the circular array (*TargetField* of $10 \times 10 \text{ cm}^2$).

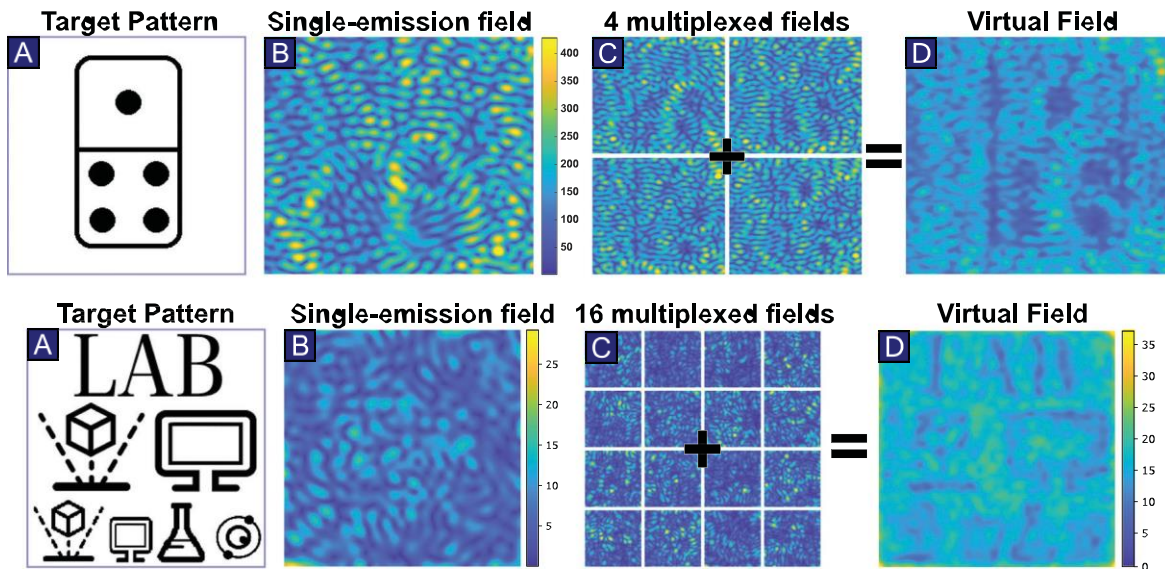


FIG. 1. (a) Target field. (b) Single-emission field. (c) Multiplexed fields. (d) Virtual field resulting from averaging the amplitude of the multiplexed fields. All fields represent amplitudes and are simulations for the (top) circular array and (bottom) square array.

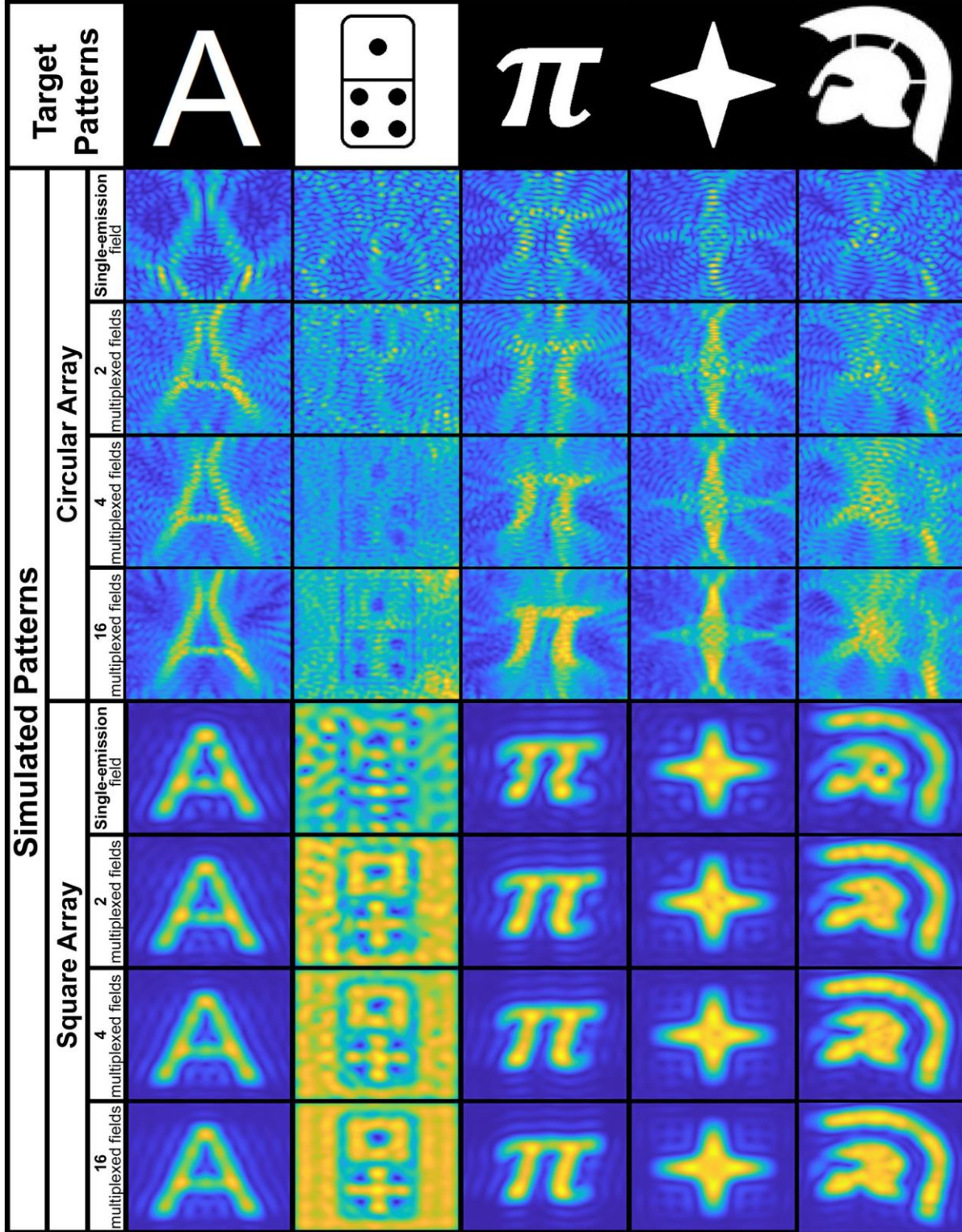


FIG. 2. Virtual fields calculated for five target patterns, for different number of multiplexed fields, for the circular and the square array. Amplitude scale bars for circular array are [0, 300] Pa and for square array are [0, 450] Pa. Fields are $10 \times 10 \text{ cm}^2$, which at 40 kHz in air represent $11.62 \times 11.62 \text{ k}$.

The arrays are shown in supplementary material Fig. 9. The operating frequency is 40 kHz; thus, the wavelength in air is approximately 8.46 mm. These arrays were selected as a representation of devices employed for particle manipulation²⁷ and patterning.³ We note that square arrays working on a target slice perpendicular to the propagation direction are the most common setup,^{2,4,8} but circular arrays are also used in patterning^{3,22} given their compact integration in the working volume. Circular arrays have marked standing wave nodes that could be mitigated and softened by averaging various multiplexed fields. We note that other geometries exist in the literature, but these two are the most representative. Virtual fields for higher-resolution arrays are shown later in the article.

The square ultrasonic array is based in the design of SonicSurface⁸ using MSO-P1040H07T (Manorshi) emitters operating at 40 kHz and of 1 cm diameter, $A_0 = 0.13$ VppPa/m $a = 5$ mm. The amplifiers were MOSFET drivers MIC4127 (Microchip) and the signals were generated by an FPGA (P4CE6E22C8N–ALTERA IV Core Board, Waveshare). The phases were sent from a PC using UART protocol at 500 kbauds and had 32 divisions per period resolution. The circular array was based on the hardware from Ultraino,²⁸ it employed MSO-A1640H10T (Manorshi) emitters operating at 40 kHz and 16 mm diameter, $A_0 = 0.36$ VppPa/m $a = 6$ mm. The drivers were TC4427A (microchip), and the signals were generated by an Arduino Mega 2560 Rev3 with a resolution of ten divisions per period. The phases were sent from a PC using UART protocol at 115 200 bauds and with an internal memory for 32 phase sets that could be emitted for specific number of periods.

Different target patterns were tested: Latin alphabet symbols, digits, and basic geometries. We report in the main paper a representative subset: letter A, as a symbol made of straight lines; an inverted domino piece, as an inverted image with straight edges and circles; the pi symbol, as a symbol with curved strokes; a star, as a simple target with straight lines and varying thickness; and a Trojan helmet, as a combination of thick and curved strokes with small gaps between them. Also, in the discussion, we show target patterns generated with arrays that have a denser distribution of emitters.

For each of the target patterns, we calculated *VirtualFields* composed of 1–16 multiplexed fields. The target patterns were

10×10 cm², discretized in fields of 256×256 points. Figure 2 shows the simulated *VirtualFields* for different target patterns grouped by array geometry.

In Fig. 2 for the circular array, the quality of the amplitude pattern gradually improves as the number of multiplexed fields increases. However, for the square array, the improvements are less noticeable beyond 2 multiplexes.

The reduction of the mean squared error (MSE) as the number of multiplexed fields increases is shown in Fig. 3 for both circular array and square array. The graphs show two different sets of lines: a dashed set, which is the MSE evolution as the virtual fields are composed of more multiplexed fields; and a solid one, representing the normalized MSE as we increase the density of emitters. For increasing the density of emitters, the dimensions of the arrays remained constant, but more emitter of smaller diameter were used, also their emitter power constant A_0 was adjusted. For example, in the 16×16 square array, emitters had 1 cm diameter and $A_0 = 0.13$, whereas the 32×32 array used 0.5 cm emitters and $A_0 = 0.0325$ (divided by 4).

The MSE drops when using a 2-field multiplexation as it was also seen in the patterns. In some cases, using virtual fields offers better quality in the resulting patterns than increasing the density of emitters (see Fig. 3). For example, for the “Trojan helmet” pattern, a circular array would need to double its emitters to obtain a result similar to the virtual field composed of six multiplexed fields; and with a square array, the quality of a virtual field is not matched with double the number of emitters. In all cases, using virtual fields improves the quality, except for the basic star pattern in the square array, which already has enough emission resolution from the array. The domino pattern in the circular array is the most significant example of how virtual fields improve the resolution of the obtained field.

In supplementary material Fig. 10, simulations for other patterns produced by the square array are shown. Additionally, simulations for a smaller 8×8 square array are shown in supplementary material Figs. 10 and 11.

The ultrasonic arrays emitted the same patterns as in the simulations for different number of multiplexed fields to experimentally scan the virtual fields. The phased-arrays were powered with 10 V and a computer sent the emissions for each of the multiplexed fields. Fields

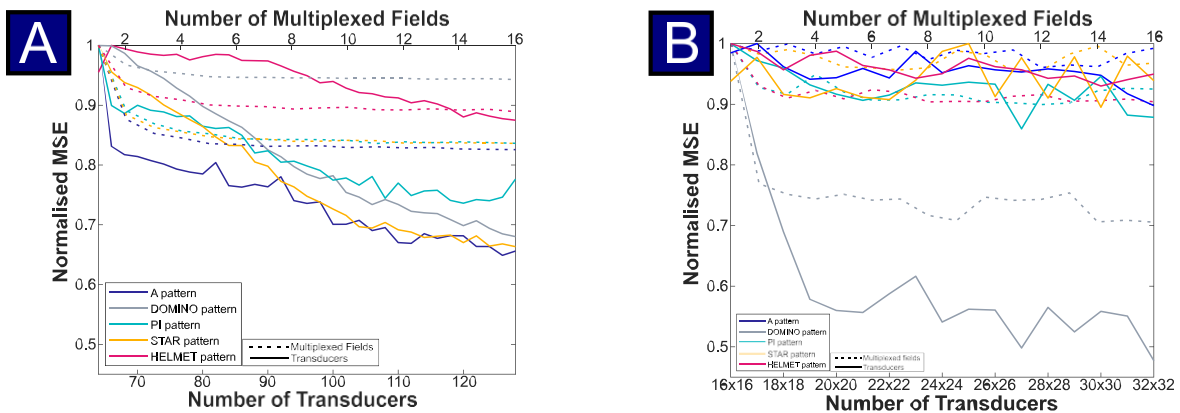


FIG. 3. Evolution of the normalized MSE of virtual fields compared with increasing the density of emitters for (a) a circular array and (b) a square array. The upper X-axis shows the number of time-multiplexed fields (dashed line), and the lower one shows the number of emitters (solid line). The MSE was normalized by dividing by its maximum value.

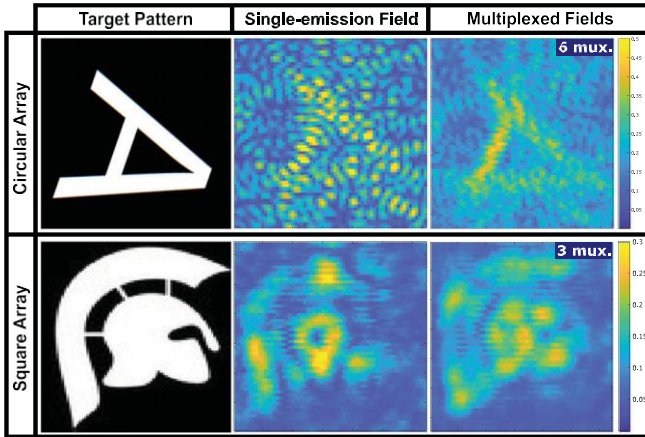


FIG. 4. Experimental scans of two patterns for a single-emission field, and 3 or 6 multiplexed fields on the circular and square arrays. They are presented as amplitude fields measured in arbitrary units.

were switched at 100 Hz, and the reported value is the RMS averaged over 5 ms. Nonetheless, other frequencies may be used, as long as the average RMS can be captured correctly from the emitted signal.

Figure 4 shows the experimental amplitude slices of the virtual fields. For both single and multiplexed fields, some details are lost between the simulated and the scanned fields. We attribute this to reflections from the scanning head as well as phase and amplitude variations of the emitters of the phased-arrays.

To scan the fields, the setups shown in supplementary material Fig. 5 were used. These setups measure slices of the acoustic pressure distribution generated by the arrays. The square array is placed directly

on the bed. The circular array is suspended in parallel to the bed at a fixed height. An ultrasonic receiver (MANORSHI 16 mm MSO-A1640H10T) is attached to the head of a delta stage (Anycubic Kossel). This receiver has a diameter of 16 mm. A PLA 3D-printed 1.5 mm diameter wide conical aperture tip is attached to the ultrasonic receiver to achieve a narrower acquisition aperture. A Matlab script communicates with the delta stage and moves the receiver to different positions with 1.5 mm spacing on a 96×96 mm grid for the square array and on a 85×85 mm grid for the circular array. At each measuring point, the computer takes samples captured by an oscilloscope (RedPitaya STEMLab 125–10) and calculates the signal's root mean square (RMS). The signal acquisition is configured to capture all the multiplexed fields. These RMS values can be translated to amplitude in arbitrary units (a.u.). The computer sends the emission phases of each multiplexed field to the arrays through the UART protocol, and it controls the stage using the G-CODE protocol.

Thermal patterns generated on a piece of fabric are shown in Fig. 5 as captured by a thermal camera (FLIR A655sc). A square array was powered with 12 V and placed 20 cm above a neoprene piece of fabric, and virtual fields were emitted for 20 s. Two target patterns were tested, with a single-emission field and with virtual fields composed of 4 and 16 multiplexed fields switched at 0.5 Hz. The variation between the coldest and hottest points is similar using single-emission or virtual fields meaning that no power loss was observed when using virtual fields, only an increase on the quality of the patterns. It is also relevant to highlight that the employed square array was not a HIFU array; thus, the observed heating is not sufficient for therapy applications. Yet, when using more powerful emitters, the patterns would be equally accurate but with a larger temperature difference. We also note that switching frequencies ranging from 1 to 100 Hz provided similar results.

Depending on the target application, the system will react as if the average of the effects of the multiplexed fields is acting on the

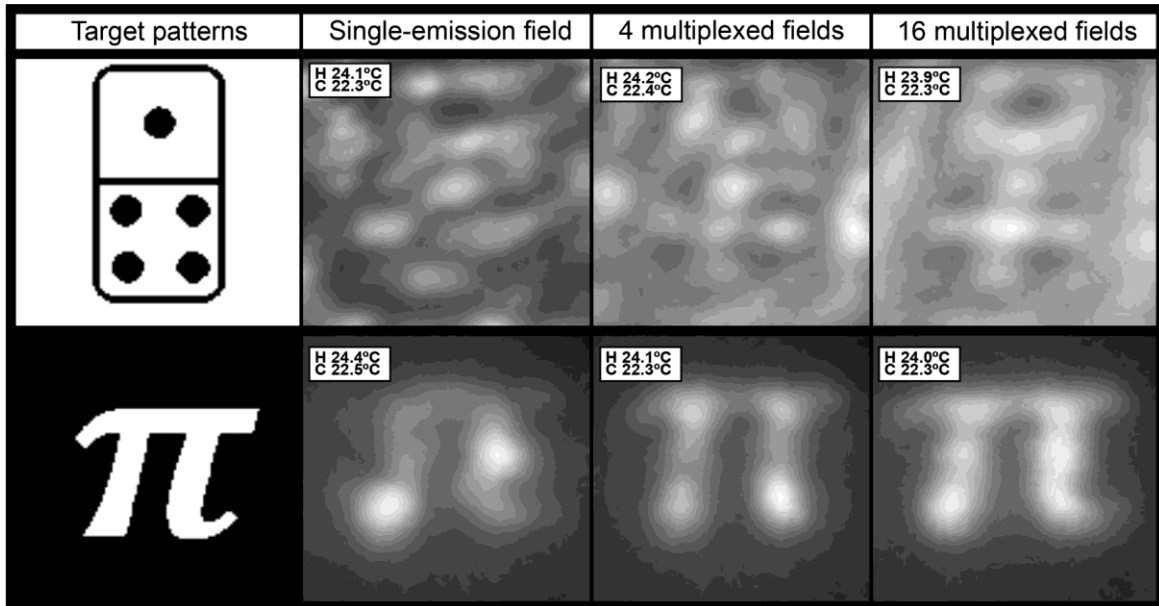


FIG. 5. Thermal images obtained for “Domino” and “Pi symbol” target patterns. The single-emission field pattern is compared to virtual fields composed of 4 and 16 multiplexed fields from the square array.

system. For example, a particle inside switching acoustic fields will perceive the average of the forces resulting from each field. Acoustic levitation in mid-air requires a switching frequency of 1 kHz²⁰ whereas manipulation in water requires less frequency.¹⁹ For thermal patterns, we switched the fields at 0.5 Hz, but faster speeds will be required if heat dissipation is large. For aerosol patterning (supplementary material Fig. 2), a multiplexation speed of 1 Hz produced a clean average between the patterns. Multiplexation speeds beyond 1 kHz will result in power loss since the emitters require some time to transition between different fields (supplementary material 3).

Most common commercially available (UltraLeap Ltd.) and DIY⁸ phased-arrays have emitter densities similar to the ones used in these experiments. Nonetheless, imaging arrays have higher densities of emitters and, in the future, it is to be expected to have high-power high-density phased-arrays; for example, in novel HIFU therapies, currently performed with static modulators.²⁹ In supplementary material Fig. 8, we show that virtual fields also improve the quality of the amplitude fields when the arrays have a high density of emitters.

In the presented results, only phase emissions were adjusted. In most arrays, it is also possible to control the emission of amplitude for each emitter, but in supplementary material Fig. 6, we show that when the target amplitude of the desired patterns reaches a certain value, having amplitude modulation does not provide better results. Regardless of that, in supplementary material Fig. 7, we show that virtual fields also improve target patterns whether amplitude modulation is available or not. For keeping the emission amplitude within a range, a cosine function was applied to it so that it would be limited to $[-1, 1]$ amplitudes where initialized with uniform distribution $[-p, p]$, on which the cosine was applied.

We have presented a technique to improve the quality of acoustic amplitude patterns. This technique has been explored for arrays commonly used for dynamic patterning and levitation; namely, a square array of 16×16 emitters, and a circular array of 12 cm radius and 64 emitters. Amplitude virtual fields obtained by time multiplexation have been presented in simulations and compared to the alternative of increasing the density of the emitters. Virtual fields have also been experimentally evaluated by scanning the fields and by capturing thermal patterns created with them. This technique improves the resolution of the produced amplitude fields without modifying the hardware and also works for upcoming high-resolution arrays. Thus, it can provide benefits in the fields of bio-printing, medical ultrasound, or parallel particle manipulation. Moreover, the method can be interesting for the terahertz community, since the wavelengths are similar and there is also a lack of spatial resolution in their emission phased arrays.

See the supplementary material for details supplementary material Figs. 1 — 11.

This research was funded by the EU Horizon 2020 research and innovation programme under Grant Agreement No. 101017746 TOUCHLESS and by the European Research Consortium under Grant Agreement No. 101042702 Intevol-ERC2021-STG.

AUTHOR DECLARATIONS

Conflict of Interest

The authors have no conflicts to disclose.

Author Contributions

Sonia Elizondo: Conceptualization (equal); Investigation (lead); Software (equal); Visualization (equal); Writing – original draft (equal); Writing – review & editing (lead). Iñigo Ezcurdia: Investigation (supporting); Software (supporting); Visualization (equal); Writing – review & editing (equal). Jaime Goñi: Conceptualization (supporting); Software (equal); Visualization (supporting). Mikel Galar: Conceptualization (supporting); Writing – review & editing (supporting). Asier Marzo: Conceptualization (equal); Funding acquisition (lead); Software (equal); Supervision (lead); Writing – original draft (equal); Writing – review & editing (equal).

DATA AVAILABILITY

The data that support the findings of this study are available from the corresponding author upon reasonable request.

REFERENCES

- 1K. Melde, A. G. Mark, T. Qiu, and P. Fischer, "Holograms for acoustics," *Nature* 537, 518–522 (2016).
- 2K. Melde, H. Kremer, M. Shi, S. Seneca, C. Frey, I. Platzman, C. Degel, D. Schmitt, B. Schölkopf, and P. Fischer, "Compact holographic sound fields enable rapid one-step assembly of matter in 3D," *Sci. Adv.* 9, eadf6182 (2023).
- 3J. M. Shapiro, B. W. Drinkwater, A. W. Perriman, and M. Fraser, "Sonolithography: In-air ultrasonic particulate and droplet manipulation for multiscale surface patterning," *Adv. Mater. Technol.* 6, 2000689 (2021).
- 4Z. Ma, A. W. Holle, K. Melde, T. Qiu, K. Poeppel, V. M. Kadiri, and P. Fischer, "Acoustic holographic cell patterning in a biocompatible hydrogel," *Adv. Mater.* 32, 1904181 (2020).
- 5D. Andrés, J. Vappou, N. Jiménez, and F. Camarena, "Thermal holographic patterns for ultrasound hyperthermia," *Appl. Phys. Lett.* 120, 084102 (2022).
- 6N. Lipsman, Y. Meng, A. J. Bethune, Y. Huang, B. Lam, M. Masellis, N. Herrmann, C. Heyn, I. Aubert, A. Boutet *et al.*, "Blood–brain barrier opening in Alzheimer's disease using MR-guided focused ultrasound," *Nat. Commun.* 9, 2336 (2018).
- 7L. Gavrilov, E. Tsurulnikov, and I. A. I. Davies, "Application of focused ultrasound for the stimulation of neural structures," *Ultrasound Med. Biol.* 22, 179–192 (1996).
- 8R. Morales, I. Ezcurdia, J. Irisarri, M. A. Andrade, and A. Marzo, "Generating airborne ultrasonic amplitude patterns using an open hardware phased array," *Appl. Sci.* 11, 2981 (2021).
- 9D. Iablonskyi, F. Sundblad, B. Wuensch, A. Klami, A. Salmi, and E. Haeggström, "Tailored acoustic holograms with phased arrays," in *IEEE International Ultrasonics Symposium (IUS)* (IEEE, 2022).
- 10Y. Xie, C. Shen, W. Wang, J. Li, D. Suo, B.-I. Popa, Y. Jing, and S. A. Cummer, "Acoustic holographic rendering with two-dimensional metamaterial-based passive phased array," *Sci. Rep.* 6, 35437 (2016).
- 11Y. Zhu, J. Hu, X. Fan, J. Yang, B. Liang, X. Zhu, and J. Cheng, "Fine manipulation of sound via lossy metamaterials with independent and arbitrary reflection amplitude and phase," *Nat. Commun.* 9, 1632 (2018).
- 12W. Li, G. Lu, and X. Huang, "Acoustic hologram of the metasurface with phased arrays via optimality criteria," *Mech. Syst. Signal Process.* 180, 109420 (2022).
- 13X.-B. Miao, H.-W. Dong, S.-D. Zhao, S.-W. Fan, G. Huang, C. Shen, and Y.-S. Wang, "Deep-learning-aided metasurface design for megapixel acoustic hologram," *Appl. Phys. Rev.* 10, 021411 (2023).
- 14X. Ren, Q. Zhou, J. Huang, Z. Xu, and X. Liu, "Holographic generation of arbitrary ultrasonic fields by simultaneous modulation of amplitude and phase," *Ultrasonics* 134, 107074 (2023).
- 15M. D. Brown, B. T. Cox, and B. E. Treeby, "Design of multi-frequency acoustic kinoforms," *Appl. Phys. Lett.* 111, 244101 (2017).
- 16Q. Lin, R. Zhang, F. Cai, Y. Chen, J. Ye, J. Wang, H. Zheng, and H. Zhang, "Multi-frequency acoustic hologram generation with a physics-enhanced deep neural network," *Ultrasonics* 132, 106970 (2023).

- ¹⁷L. Cox, K. Melde, A. Croxford, P. Fischer, and B. W. Drinkwater, "Acoustic hologram enhanced phased arrays for ultrasonic particle manipulation," *Phys. Rev. Appl.* 12, 064055 (2019).
- ¹⁸A. G. Athanassiadis, L. Schlieder, K. Melde, V. Volchkov, and P. Fischer, "Animating sound using neurally multiplexed holograms," *J. Acoust. Soc. Am.* 148, 2807–2807 (2020).
- ¹⁹P. Glynne-Jones, R. J. Boltryk, N. R. Harris, A. W. Cranny, and M. Hill, "Mode-switching: A new technique for electronically varying the agglomeration position in an acoustic particle manipulator," *Ultrasonics* 50, 68–75 (2010).
- ²⁰A. Marzo, M. Caleap, and B. W. Drinkwater, "Acoustic virtual vortices with tunable orbital angular momentum for trapping of Mie particles," *Phys. Rev. Lett.* 120, 044301 (2018).
- ²¹L. Cox, A. Croxford, B. Drinkwater, and A. Marzo, "Acoustic lock: Position and orientation trapping of non-spherical sub-wavelength particles in mid-air using a single-axis acoustic levitator," *Appl. Phys. Lett.* 113, 054101 (2018).
- ²²L. Cox, A. Croxford, and B. W. Drinkwater, "Dynamic patterning of microparticles with acoustic impulse control," *Sci. Rep.* 12, 14549 (2022).
- ²³A. Watanabe, K. Hasegawa, and Y. Abe, "Contactless fluid manipulation in air: Droplet coalescence and active mixing by acoustic levitation," *Sci. Rep.* 8, 10221 (2018).
- ²⁴F.-S. Lin, P.-W. Yang, C.-C. Hsieh, H.-Y. Su, L.-X. Chen, C.-Y. Li, and C.-H. Huang, "Investigation of a novel acoustic levitation technique using the transition period between acoustic pulse trains and electrical driving signals," *IEEE Trans. Ultrason., Ferroelectr., Freq. Control* 69, 769–778 (2022).
- ²⁵R. Hirayama, D. Martinez Plasencia, N. Masuda, and S. Subramanian, "A volumetric display for visual, tactile and audio presentation using acoustic trapping," *Nature* 575, 320–323 (2019).
- ²⁶H. O'Neil, "Theory of focusing radiators," *J. Acoust. Soc. Am.* 21, 516–526 (1949).
- ²⁷A. Marzo and B. W. Drinkwater, "Holographic acoustic tweezers," *Proc. Natl. Acad. Sci. U. S. A.* 116, 84–89 (2019).
- ²⁸A. Marzo, T. Corkett, and B. W. Drinkwater, "Ultraino: An open phased-array system for narrowband airborne ultrasound transmission," *IEEE Trans. Ultrason., Ferroelectr., Freq. Control* 65, 102–111 (2018).
- ²⁹D. Andrés, N. Jiménez, J. M. Benlloch, and F. Camarena, "Numerical study of acoustic holograms for deep-brain targeting through the temporal bone window," *Ultrasound Med. Biol.* 48, 872–886 (2022).